Journal of Structural Geology, Vol. 15, No. 8, pp. 995 to 1006, 1993
Printed in Great Britain

0191-8141/93 $06.00+0.00

Deformation conditions in the northern Subalpine Chain, France, estimated from deformation modes in coarse-grained limestone

DAVID A. FERRILL* and RICHARD H. GROSHONG, JR

Department of Geology, The University of Alabama, Tuscaloosa, AL 35487-0338, U.S.A.

(*Received* 19 *July* 1991; *accepted in revised form* 19 *October* 1992)

Abstract—In low-temperature experiments, the deformation mode and ductility in a single rock type are most directly controlled by the confining pressure and strain magnitude. A graphical technique is developed from published experimental microstructural data that allows for the determination of deformation mode for coarse-grained limestone on the basis of microstructural point-count data. The deformation mode and strain are used to constrain the confining pressure during thin-section scale deformation by comparison with experimental deformation results. The technique is applied to coarse-grained samples of Cretaceous and Tertiary limestone from the northern Subalpine Chain, France, and reveals that the majority of samples deformed mostly by twinning in the uniform flow mode at minimum depths, estimated from deformation mode and strain, of between 0 and 6.0 km and maximum depths, interpreted from peak metamorphic temperatures and geothermal gradient, of about 2.7–9.7 km. In the remaining samples, brittle failure probably occurred at relatively shallow depths (<2.5 km) or in response to lowered effective confining pressure due to elevated fluid pressures.

INTRODUCTION

CONFINING pressure is one of the principal environmental controls on the internal (thin-section scale) deformation of rocks at low temperature (Handin 1966, Donath 1970, Donath *et al.* 1971). It is, however, difficult to determine directly the confining pressure of natural low-temperature deformation. Confining pressure estimates are generally calculated from depth estimates using an assumed pressure–depth gradient (Donath 1970, Hyndman 1985). Two methods are commonly employed to estimate the depth: (a) metamorphic indicators, such as vitrinite reflectance, illite crystallinity or conodont color alteration, are used to estimate the maximum temperature, then the depth is calculated assuming a reasonable geothermal gradient (Groshong 1975, Spang & Groshong 1981, Burkhard & Kalkreuth 1989, Evans & Dunne 1991); or (b) overburden thickness is projected from a nearby area where the thickness can be measured (Groshong 1975, Spang & Groshong 1981). There are several problems with using these maximum burial estimates to calculate the confining pressure during deformation. First, the internal (thin-section scale) deformation may not have coincided with maximum burial. Second, the low-temperature metamorphic indicators are most sensitive to temperature. The peak temperature may not simply be due to the burial depth but also may be increased by overthrusting of a hot thrust sheet (Yonkee *et al.* 1989), passage of hot fluids through the rock, internal strain heating or shear heating along a major décollement (Barr & Dahlen 1989). Estimates based on metamorphic temperature may, therefore, overestimate the depth. If rapid exhumation occurs before the temperature stabilizes, then estimates based on metamorphic temperature may underestimate the depth. Third, the geothermal gradient is usually unknown and estimates based on incorrect gradients will over- or underestimate the depth. Fourth, the effective confining pressure may have been lowered by elevated pore fluid pressure (Secor 1965, Engelder 1985, Hancock 1985). Depths and confining pressures estimated from temperature estimates are still in many cases the most reliable data and will be used as a constraint for the maximum confining pressure and depth in the present paper. The goal of the present paper is to constrain the pressure and depth of thin-section scale deformation within the range from surface conditions to maximum burial.

It would be useful to have a technique for estimating the confining pressure that is sensitive to the conditions during the internal deformation only. Experimental data illustrate that in low-temperature deformation, the deformation mechanisms, deformation mode, and ductility depend directly on the confining pressure (Donath 1970). The approach taken here is to extrapolate the results of experimental deformation studies to natural deformation by comparing the deformation mechanisms, deformation modes and ductility of the experimentally deformed rocks and naturally deformed rocks as suggested by Donath *et al.* (1971). The confining pressure of deformation for naturally deformed rocks can be inferred based on the confining pressure for analogous experimentally deformed rocks.

A deformation mode is the macroscopic expression (visible in hand sample) of the microscopic and submicroscopic deformation (Donath *et al.* 1971), and ductility is the percent permanent strain before failure by fracture or faulting (Handin 1966, Donath *et al.* 1971). Deformation mode and ductility depend upon rock type and

*Present address: Shell Offshore Inc., Exploration Department, P.O. Box 61933, New Orleans, LA 70161, U.S.A.

the environmental conditions: confining pressure, temperature, strain rate, strain magnitude, pore fluids and pore fluid pressure (Heard 1963, Donath 1970, Donath & Fruth 1971). Confining pressure increase, temperature increase and the presence of chemically active pore fluids tend to increase ductility (Handin 1966, Donath 1970). Increased strain rates and increased pore fluid pressures tend to decrease ductility (Handin 1966, Donath 1970). By holding the rock type constant, the differences in deformation mode can be attributed to differing environmental conditions.

In general, it is considered difficult to extrapolate experimental rock deformation results to naturally deformed rocks, largely because of the differences between the geological and experimental strain rates. However, experimental data for limestone and marble deformed at strain rates equal to or less than 10^{-3} and temperatures below 400°C indicate that the ductility is largely independent of the strain rate, especially under conditions where the failure mode is brittle faulting (Donath 1970, Donath & Fruth 1971, Rutter 1974). The presence of pore fluids is generally unimportant to the deformation modes and ductility in low-temperature deformation unless syntectonic compaction occurs to elevate the fluid pressure or the fluid acts as an agent in pressure solution (Secor 1965, Rutter 1974, Groshong 1988). At shallow depths (<10 km), deformation mode and ductility are most directly controlled by the confining pressure and strain magnitude (Donath 1970, Donath *et al.* 1971).

Experimental deformation of oolitic Crown Point Limestone (Donath 1970, Donath *et al.* 1971, Tobin & Donath 1971) at room temperature, dry, at confining pressures from 0.1 to 200 MPa and a strain rate of $3.9 \times 10^{-5}\ s^{-1}$ to total strains of 0.52–23.32%, showed that the deformation modes change systematically with confining pressure and total strain. Deformation modes defined from the macroscopic observation of experimentally deformed cylinders of limestone (Donath 1970, Donath *et al.* 1971) are extension fracture, brittle faulting, ductile faulting, incipient ductile faulting and uniform flow. Failure is recognized by the onset of falling stress with increasing strain. The uniform flow mode is characterized by deformation without failure and strain occurring dominantly by twinning (Tobin & Donath 1971). Beyond the ultimate rock strength, failure occurs by one of the other deformation modes. The extension fracture mode is characterized by fractures parallel to the principal compression direction and extension perpendicular to the fractures. The brittle faulting mode is defined by localized offset where cohesion is lost across a shear fracture or zone. Ductile faulting, in contrast, is defined by localized offset without loss of cohesion across a zone of velocity discontinuity in flow (Donath 1970). Incipient ductile faulting is defined by failure before a ductile fault is macroscopically visible. On a graph of total strain vs confining pressure (Fig. 1), the boundary between the uniform flow mode and the various failure modes is the ductility curve.

If the deformation mode and strain are known for

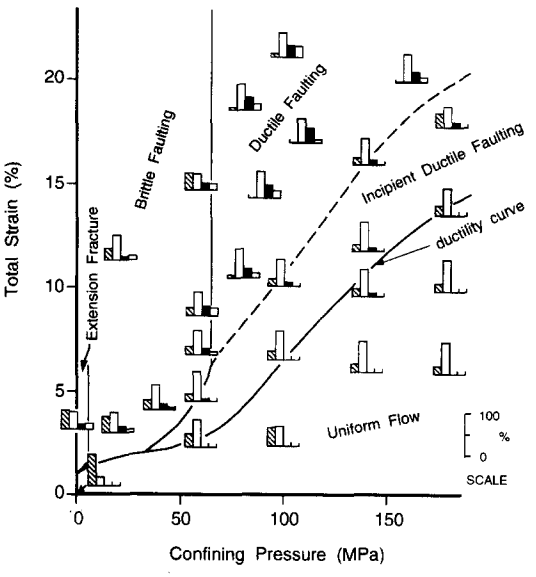

Fig. 1. Deformation mode field diagram from Tobin & Donath (1971) with microstructural data presented as histograms. Columns 1, 2 and 3 (left to right) represent normalized percentages of calcite grains that are: (1) undeformed (U); (2) twinned only (T); or (3) twinned and fractured or faulted (T + F), respectively. The fourth column represents all grains counted in the rock that were cut by transgranular fractures or faults. The samples were deformed at room temperature, dry, at confining pressures from 0.1 to 200 MPa and a strain rate of $3.9 \times 10^{-5}\ s^{-1}$ to total strains of 0.52–23.32%.

experimentally deformed coarse-grained limestones, confining pressure can be inferred from the confining pressure vs strain deformation mode diagram (Donath 1970, Donath *et al.* 1971, Wu 1989). Strain in coarse-grained limestone is commonly measured either using strain markers such as ooids or pellets for shape and orientation (e.g. Dunnet 1969) or distribution analysis (e.g. Fry 1979) to determine the finite strain (Ramsay & Huber 1984), or using twins in calcite cement or fossils to calculate the twinning strain (Groshong 1972, 1974). If the strain is known, the problem is reduced to determining the deformation modes. Deformation modes in naturally deformed limestone have previously been interpreted visually with the same goal in mind; namely determining the confining pressure and depth of deformation (Wu 1989). In the present study, microstructural data for each of the experimental deformation modes (Tobin & Donath 1971) are inverted to define the deformation modes according to microstructure so as to ascertain that the deformation mechanisms and modes in the naturally and experimentally deformed limestones are directly analogous. Microstructural data are then used to determine the deformation modes for naturally deformed limestone from the northern Subalpine Chain (France) which are then used with calcite twin strain data to help constrain the confining pressures and depths of deformation by comparison with the deformation mode diagram of Donath *et al.* (1971).

MICROSTRUCTURAL DEFORMATION-MODE DIAGRAM

Statistical analysis of microstructural point count data from experimentally deformed coarse-grained lime-

stone (Tobin & Donath 1971) revealed that the different deformational modes were best characterized microstructurally on the basis of four categories of grains (Fig. 1). Three of the categories are grains that are: (1) undeformed; (2) twinned (*e*-twins); and (3) twinned and fractured or faulted. The percentages of coarse grains for these three categories are normalized to 100% so that slightly different rock types can be directly compared (Tobin & Donath 1971). Category (4) is a whole-rock percentage representing grains cut by transgranular discontinuities (extension fractures or faults). Tobin & Donath (1971) concluded that three of the four microstructural categories of coarse grains were useful in actually distinguishing the deformational modes: (1) undeformed grains; (2) twinned and fractured or faulted grains; and (3) transgranular discontinuities. The uniform flow and incipient ductile faulting modes are characterized microstructurally by a near total absence of transgranular extension fractures or faults (0–0.3%). The incipient ductile faulting mode has higher percentages of grains with twins and extension fractures or faults (7.3–14.3%) than does the uniform flow mode (0.6–7.0%; Fig. 1). The ductile faulting and brittle faulting modes have transgranular discontinuity percentages of 6.5–25.2%. The microstructural characteristics of the single extensional fracturing sample (Fig. 1) are virtually indistinguishable from the brittle faulting samples. Therefore, the extension fracture sample is included with the brittle faulting mode (Tobin & Donath 1971). The brittle faulting samples are distinguished from the ductile faulting samples by having much greater percentages of undeformed grains: 20.3–45.6% for brittle faulting vs 3.4–12.5% for ductile faulting.

In order to define uniquely the deformation modes graphically on the basis of the microstructures, the three microstructural categories that Tobin & Donath (1971) determined could distinguish the deformation modes are used to define the axes of a graph (Fig. 2). The transgranular extension fracture and fault percentage is plotted vs the percentage of grains with twins and fractures or faults (T + F) divided by the percentage of undeformed (U) grains. The transgranular extension fractures or faults percentage separates the brittle faulting and ductile faulting samples from the uniform flow and incipient ductile faulting samples. The (T + F)/U axis separates the uniform flow samples from the incipient ductile faulting samples because the uniform flow samples have fewer grains with twins and fractures or faults. The brittle faulting samples are separated from the ductile faulting samples by the considerably greater abundance of undeformed grains in the brittle faulting samples. Using the transgranular fractures or faults percentage and (T + F)/U for the axes gives the best separation of the modes on a binary graph. To spread the data along the (T + F)/U axis, a four-cycle log scale is used. All (T + F)/U values between 0 and 0.01 are plotted at 0.01. The resulting graph yields uniquely defined deformation mode fields without data overlap (Fig. 2). The boundaries between the deformation mode fields are shown using straight lines that evenly split the data gaps and the area of the data gap is shaded (Fig. 2). More precise placement of the boundaries would depend on additional experimental data. This graph will be used to define the macroscopic deformation modes for naturally deformed limestone from the northern Subalpine Chain.

APPLICATION TO THE NORTHERN SUBALPINE CHAIN

Study area

The northern Subalpine Chain of Haute-Savoie, France, is a fold-dominated fold–thrust belt consisting of Mesozoic and Cenozoic sedimentary strata located between the Molasse Basin to the northwest and external basement massifs to the southeast (Collet 1927) (Fig. 3). The northern Subalpine Chain is structurally beneath the Prealps, which were emplaced by the Pennine thrust (Collet 1927) that has since been eroded leaving klippen of the Prealps. The uppermost stiff lithotectonic unit and the best exposed unit in the northern Subalpine Chain is the Cretaceous Urgonian Limestone (approximately 200 m thick; Charollais *et al.* 1977). The Urgonian Limestone was chosen for study because it is coarse grained, allowing for twin strain analysis and because it is well exposed across the width of the fold–thrust belt which allowed for sampling of the Urgonian Limestone through the range of metamorphism in the area (Ferrill 1991a).

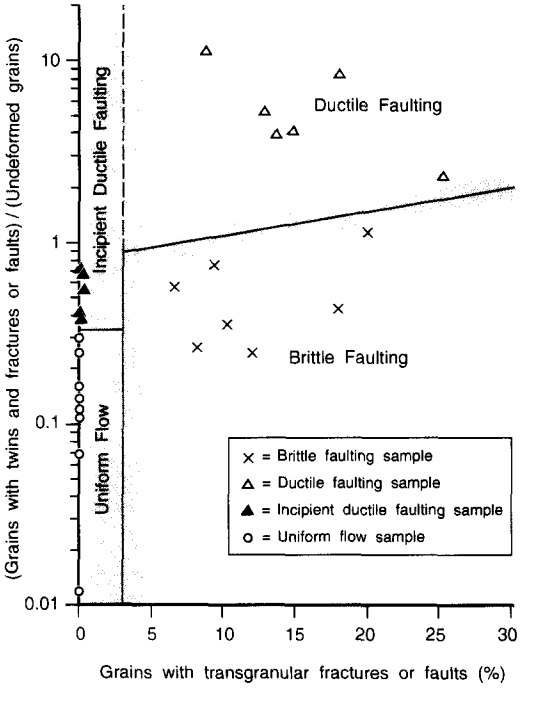

Fig. 2. Inverted deformation mode field diagram derived using microstructural data of Tobin & Donath (1971). The horizontal axis represents the grains cut by transgranular discontinuities (extension fractures or faults). The vertical axis is the percentage of grains with twin lamellae and fractures or faults (T + F) divided by the percentage of undeformed grains (U). All values of (T + F)/U between 0 and 0.1 are plotted at 0.01.

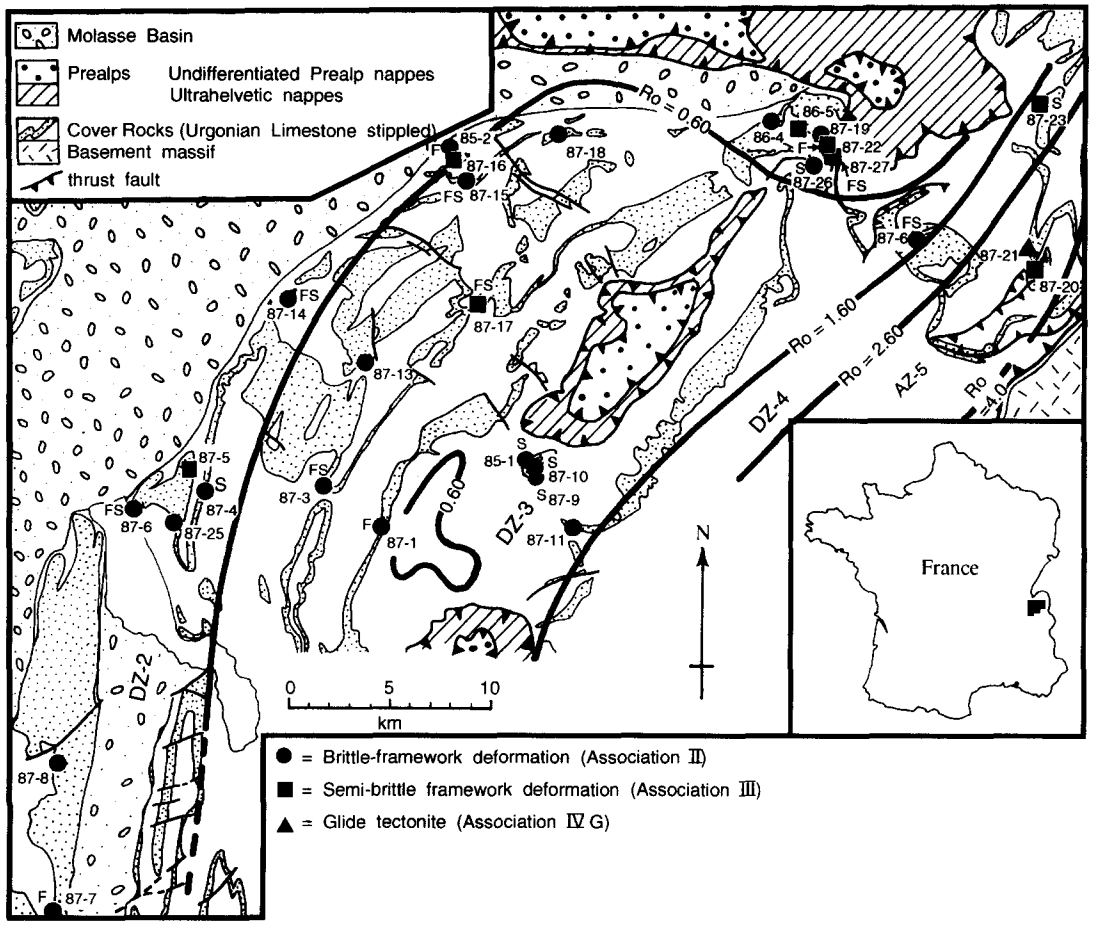

Fig 3. Geologic map of the northern Subalpine Chain (after Goguel 1966, Ricour *et al.* 1969) showing locations for the 29 samples, and metamorphic zone boundaries (*Ro* = 0.60, 1.60, 2.60 and 4.0; Table 1). Sample 86-5 is Hauterivian Limestone, samples 85-1 and 86-6 are Eocene limestone, and the remaining samples are Urgonian Limestone. Symbols used to mark the samples from different deformation-mechanism associations (Groshong 1988) are annotated using F and S to indicate samples having more than 3% grains cut by fractures (extension veins or faults; F), or pressure-solution surfaces (S). Diagenesis zone 2 (DZ-2) is between vitrinite reflectance values (*Ro*) of 0.3 and 0.6, diagenesis zone 3 (DZ-3) between 0.6 and 1.6, diagenesis zone 4 (DZ-4) between 1.6 and 2.6, and anchizone (AZ-5) between 2.6 and 4.0 (Kübler *et al.* 1979). The locations of metamorphic boundaries (after Kübler *et al.* 1979) are based on vitrinite reflectance data and illite crystallinity data from Kübler *et al.* (1979) and Aprahamian & Pairis (1981), combined using the equation of Guthrie *et al.* (1986) which converts illite crystallinity data (Kübler index) to equivalent vitrinite reflectance values.

Metamorphism

The term metamorphism as used here includes any type of mineralogical change including diagenesis (Kübler *et al.* 1979). Published vitrinite reflectance (Kübler *et al.* 1979), illite crystallinity (Kübler *et al.* 1979, Aprahamian & Paris 1981) and metamorphic mineral assemblage data (Kübler *et al.* 1979) for the northern Subalpine Chain indicate an increase in metamorphism from low-temperature diagenesis at the front of the belt through anchimetamorphism (see Table 1) in the internal part of the northern Subalpine Chain (Fig. 3). The metamorphism is generally thought to be due to burial by the Prealps (Kübler *et al.* 1979, Aprahamian & Pairis 1981).

Metamorphic-zone boundaries in the study area are placed using published vitrinite reflectance and illite crystallinity data (Kübler *et al.* 1979, Aprahamian & Pairis 1981), and using the values for the zone boundaries of Kübler *et al.* 1979) (Fig. 3). The metamorphic zones represented are diagenesis zones (DZ) 2, 3 and 4 and anchizone 5 (AZ5). Maximum temperatures for the boundaries are interpreted using empirical temperature and mean vitrinite reflectance data from four boreholes, drilled for geothermal energy in the Rhine Graben, with geothermal gradients of 44–77°C km^{-1} (fig. 9 of Teich-

Table 1. Maximum temperature, depth and confining pressure interpreted for the Subalpine Chain metamorphic boundaries (Fig. 3). *Ro* values are mean vitrinite reflectance values for boundaries between diagenesis zone 2 (DZ-2), diagenesis zone 3 (DZ-3), diagenesis zone 4 (DZ-4) and anchizone (AZ-5) after Kübler *et al.* (1979). Temperature ranges for boundaries are from Frey (1986) (upper anchizone boundary) and fig. 9 in Teichmüller (1987). Frey (1986) estimates the temperature for the diagenesis–anchizone boundary to be 200°C. Depths calculated assuming a surface temperature of 10°C (Yonkee *et al.* 1989), and a geothermal gradient of 30°C km^{-1} (Sawatzki 1975, Aprahamian & Pairis 1981). Confining pressure was calculated from depth assuming a pressure gradient of 26.0 MPa km^{-1} (after Hyndman 1985)

Boundaries	*Ro*	Temperature (°C)	Depth (km)	Pressure (MPa)
Lowest value	0.43	55–105	1.5–3.2	39.0–83.2
DZ2-DZ3	0.60	90–125	2.7–3.8	70.2–98.8
DZ3-DZ4	1.60	150–170	4.7–5.3	122.2–137.8
DZ4-AZ	2.60	170–190	5.3–6.0	137.8–156.0
Upper AZ	4.00	300	9.7	252.2

müller 1987). For this wide range of geothermal gradients, Teichmüller (1987) found the best correlation was between the mean vitrinite reflectance and temperature rather than between vitrinite reflectance and thermal gradient or depth. This temperature–vitrinite reflectance correlation is used here to estimate temperatures for the metamorphic-zone boundaries. The range of peak metamorphic temperature estimated for each boundary is as follows: DZ2–DZ3 = 90–125°C; DZ3–DZ4 = 150–170°C; DZ4–AZ5 = 170–190°C (Table 1). The temperature for the boundary between diagenesis zone 4 (DS-4) and anchizone (AZ-5) may be as high as 200°C, and the upper AZ-5 boundary is at around 300°C (Frey 1986, Burkhard & Kalkreuth 1989, Mosar 1989). Maximum burial depths, estimated from the peak metamorphic temperatures using the geothermal gradient of 30°C km^{-1} estimated for the northern Subalpine Chain (Sawatzki 1979, Aprahamian & Pairis 1981) and a surface temperature of 10°C (Yonkee *et al.* 1989), are in the range of 1.5–5.3 km for the DZ-2 and DZ-3 samples, and 4.7–9.7 km for the DZ-4 and AZ-5 samples (Table 1). Maximum confining pressures were calculated from the estimated depths using a pressure–depth gradient of 26.0 MPa km^{-1} assuming an average density of 2.65 g cm^{-3} for the structurally overlying limestone- and shale-dominated Prealps (Dobrin 1976, Hyndman 1985, Mosar 1988, 1989). The maximum confining pressures are estimated to be between 39.0 and 137.8 MPa for the DZ-2 and DZ-3 samples, and 122.2–252.2 MPa for the DZ-4 and AZ-5 samples (Table 1).

Sampling

Twenty-nine oriented samples of grainstone and packstone (26 from the Urgonian Limestone, one from the underlying Hauterivian Limestone, and two samples of Eocene limestone) are used in the present study (Fig. 3). The samples were collected with a wide aerial distribution (across-strike width as much as 19 km, along-strike length of 70 km) to represent the range of metamorphic grades and the regional deformation in the area. Samples were specifically chosen to avoid the local deformation associated with fold hinges and faults (except for sample 87-26, near to a fault of unknown displacement). Two bedding-perpendicular thin sections were cut from each sample (one parallel to strike and one parallel to dip) for the calcite strain-gauge analysis as recommended by Groshong *et al.* (1984b).

Point-count data

Point counting of 300–350 points was performed on the dip-parallel thin section from each sample, using the categories listed in Table 2. The microstructures in the strike and dip sections for each sample were qualitatively compared and found to be consistent (Ferrill 1991b). The categories (Table 2) were subdivided on the basis of the microstructural characteristics of coarse calcite grains (undeformed; twinned; cut by extension veins, faults, or stylolites) (Figs. 4 and 5). The data for the coarse calcite cement and fossils were separated into the microstructural categories of Tobin and Donath (1971) (Table 3). No porosity was observed in the samples. For the total number of points counted of 300–350 per sample, all percentages counted are estimated to be within ± 5.75% of the actual area percentage (95% confidence) (Plas & Tobi 1965). The only microstructures common to all samples are calcite *e*-twins. Veins and pressure-solution surfaces are present in many samples and microfaults were only observed in thin sections of one sample (87-17) (Ferrill 1991b, Ferrill & Groshong 1993). Mutual cross-cutting relationships of veins and pressure-solution surfaces in many samples suggest coeval formation, similar to observations from the Upper and Lower Glarus nappe complex in the Helvetic Alps (Groshong *et al.* 1984a). Increased crystal-plastic strain in the form of more twins and bent twins immediately adjacent to a bedding-perpendicular stylolite in one sample (87-1) suggests locally simultaneous twinning and pressure solution. No coarse-calcite filled veins were found to lack twins. Incipient recrystallization along some grain boundaries in one anchizone sample (87-20) suggests relatively high deformation temperature, *ca* 250°C (Groshong *et al.* 1984a, Evans & Dunne 1991, Burkhard 1993).

Table 2. Categories of rock components in point counting. Each category, with the exception of micrite and microspar, is subdivided on the basis of whether the calcite is twinned or untwinned. Each category is then subdivided on the basis of whether the grains are cut by faults, extension fractures (veins) or stylolites, and whether the features are parallel (±15°), perpendicular (±15°), or oblique to bedding. Ghost fabric veins are discussed by Groshong (1988, p. 1336)

1. Grains
   - A. Micrite
   - B. Microspar
   - C. Coarsely crystalline fossil (>0.06 mm)
   - E. Finely crystalline fossil (<0.06 mm)
   - F. Other grains according to rock (fibrous fossils, replacement dolomite or silica, quartz)
2. Intraparticulate material
   - A. Drusy calcite cement (<0.06 mm)
   - B. Blocky calcite cement (>0.06 mm)
3. Interparticulate material
   - A. Micrite
   - B. Microspar
   - C. Drusy cement (<0.06 mm)
   - D. Blocky cement (>0.06 mm)
   - E. Syntaxial rim cement
   - F. Replacement dolomite
4. Structural features
   - A. Drusy-fill vein (<0.06 mm)
   - B. Blocky-fill vein (>0.06 mm)
   - C. Ghost fabric vein
   - D. Fault zone
   - E. Stylolite

Twin strain

Twinning on the *e* plane is the most important crystal-plastic deformation mechanism in calcite deformed at low temperature because it requires the lowest shear stress to be activated (Turner 1953, Heard 1963, Carter & Raleigh 1969). In naturally deformed coarse-grained limestones from the Helvetic Alps deformed at less than 270°C (Groshong *et al.* 1984a) and from the Central Appalachian Valley and Ridge Province deformed at

Table 3. Microstructural data for Subalpine Chain samples. Twin strain is the second invariant of strain used here as a measure of the total distortion by twinning (after Groshong *et al.* 1984a). Deformation-mechanism associations are: brittle framework deformation (II); semi-brittle framework deformation (III); and glide tectonite (IVG) (Groshong 1988). F and S are used to signify that more than 3% of the grains are cut by extension veins or faults (F) or pressure-solution surfaces (S). Zone refers to the metamorphic zone for each sample (see Fig. 3 for locations). Rock % coarse refers to the volume percentage of the rock consisting of coarse calcite. The U (undeformed), T (twinned) and T + F (twinned and fractured or faulted) values are normalized percentages of the coarse fraction of the rock. (T + F)/U is used in defining the deformation modes (Fig. 8). Total (%) F is the percentage of counted grains cut by transgranular extension fractures or faults. Mode refers to deformation mode (from Fig. 8)

	Twin Strain											
Sample	LDR	PEV	NEV	Deformation-mechanism association	Zone	Rock % coarse	U (%)	T (%)	T + F (%)	(T + F)/U	Total F (%)	Mode
85-1	1.41			IIS	DZ-3	29.41	89.00	11.00	0.00	0.000	0	UF
85-2	0.13	0.79	0.44	IIF	DZ-2	32.22	86.62	11.33	2.05	0.024	7.64	BF
86-4	1.31			II	DZ-2	33.01	69.61	30.39	0.00	0.000	0	UF
86-5	3.21			III	DZ-2	28.51	74.15	25.85	0.00	0.000	0	UF
86-6	1.31			IIFS	DZ-3	14.83	64.23	35.77	0.00	0.000	6.99	BF
87-1	0.33			IIF	DZ-3	14.40	66.67	31.11	2.22	0.033	4.8	BF
87-3	0.97			IIFS	DZ-3	20.14	52.47	45.91	1.62	0.031	3.84	BF
87-4	0.73	5.14	1.01	IIS	DZ-2	50.83	17.04	82.96	0.00	0.000	0	UF
87-5	2.75			III	DZ-2	23.47	37.50	62.50	0.00	0.000	0	UF
87-6	0.88			IIFS	DZ-2	22.16	74.48	21.47	4.05	0.054	14.81	BF
87-7	1.31			IIF	DZ-2	43.53	36.66	62.58	0.76	0.021	7.64	BF
87-8	1.50			II	DZ-2	53.48	46.05	53.95	0.00	0.000	0.64	UF
87-9	1.15			IIS	DZ-3	29.70	47.87	52.13	0.00	0.000	0	UF
87-10	0.78			IIS	DZ-3	19.21	59.67	40.33	0.00	0.000	1.92	UF
87-11	0.24			II	DZ-3	20.89	68.17	31.83	0.00	0.000	0.32	UF
87-13	0.87			II	DZ-3	29.38	58.51	41.49	0.00	0.000	0	UF
87-14	1.43			IIFS	DZ-2	28.30	27.10	71.73	1.17	0.043	4.18	BF
87-15	1.40			IIFS	DZ-3	25.62	35.03	57.18	7.78	0.222	13.45	BF
87-16	2.68			III	DZ-2	39.66	29.85	68.76	1.39	0.047	2.48	UF
87-17	2.67			IIIFS	DZ-3	29.64	52.25	36.34	11.42	0.219	6.07	BF
87-18	0.50			II	DZ-3	31.06	64.23	35.77	0.00	0.000	1.97	UF
87-19	0.64			II	DZ-2	20.39	60.32	39.68	0.00	0.000	0	UF
87-20	4.95	12.47	10.96	III	AZ-5	20.46	14.08	85.92	0.00	0.000	0.32	UF
87-21	12.48	17.25	16.97	IVG	AZ-5	27.51	38.86	61.14	0.00	0.000	0	UF
87-22	2.46			IIIF	DZ-2	33.75	75.23	23.88	0.89	0.012	6.89	BF
87-23	4.41	7.52	4.66	IIIS	DZ-4	26.91	42.16	57.84	0.00	0.000	0	UF
87-25	0.28			II	DZ-2	16.78	88.68	11.32	0.00	0.000	1.9	UF
87-26	1.07	6.59	1.11	IIS	DZ-2	22.06	36.10	62.26	1.64	0.045	2.6	UF
87-27	6.00			IIIFS	DZ-2	12.82	77.22	22.78	0.00	0.000	5.54	BF

between 250 and 350°C (Evans & Dunne 1991), twinning dominated the intragranular deformation and accounts for 67–100% of the intragranular strain. In the Prealps Medianes Plastiques deformed at <300°C, Mosar (1989) found that strains measured using deformed pellets and calcite twin strains are about the same. Deformation in the uniform flow mode is principally accommodated by intragranular mechanisms (Donath *et al.* 1971). The twinning strain should, therefore, reasonably estimate the intragranular strain and the prefailure strain in coarse-grained limestones deformed at low temperatures.

Strain by mechanical *e*-twinning of calcite was calculated for the Subalpine Chain limestone samples using the strain-gauge technique of Groshong (1972, 1974). Strain calculations were made using 60 twin sets per sample (30 sets per thin section for two bedding-perpendicular thin-sections, one parallel to dip and the other parallel to strike), the inner width for thick twins, and a twinned material ratio of 0.5 for thin twins (Groshong 1974). Two cleaning procedures were used to improve the precision and accuracy of the strain measurements (Ferrill 1991a, Ferrill & Groshong 1993). In the first procedure (largest deviations removed; LDR), the 20% of the twin sets having the largest deviations from the calculated strain tensors were discarded to eliminate grains with the largest measurement errors and inhomogeneously deformed grains (Groshong 1974, Groshong *et al.* 1984b). For samples in which one-third or more of the twin sets had negative expected values (opposite sense of shear to that expected for calculated strain tensors), a second procedure was used. The second cleaning procedure consists of separating the twin sets with negative expected values (NEV) from those with positive expected values (PEV) in the original data sets. Each sub-set was then cleaned by removing the one to three grains (less than 7% of the grains) with the largest deviations. Calcite-twin strains are here given as the square root of the second strain invariant (Jaeger & Cook 1979, Groshong *et al.* 1984a, Ferrill 1991a) and for the LDR procedure range from 0.13 to 12.48% (Table 3). Strains calculated for the PEV and NEV data are as large as 17.25 and 16.97%, respectively. In the northern Subalpine Chain data set (samples for which the NEV and PEV data were separated) both the NEV and PEV strains are larger than the LDR strain. Therefore, the LDR strain should be considered to be the minimum twin strain. The twin strain is used here as an estimate of the prefailure strain for the uniform flow samples. The samples that failed may have continued to twin after failure (indicated by twinned vein calcite), and therefore the twinning strain may overestimate the prefailure strain.

Samples having large numbers of negative expected

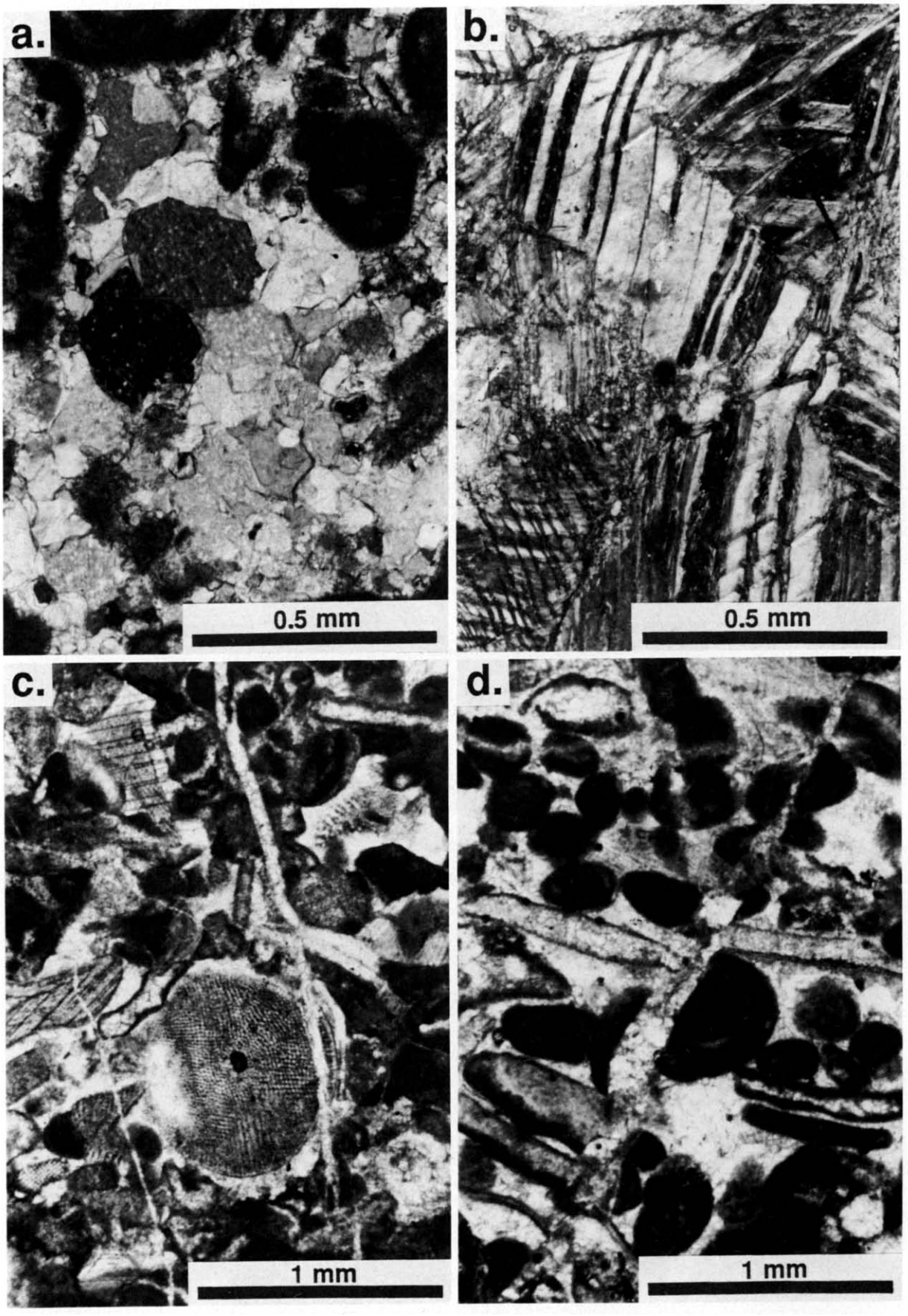

Fig. 4. Photomicrographs showing examples of microstructures used to define deformation modes: (a) undeformed grains and cement (sample 87-25, 0.28% LDR twin strain); (b) thick twins in calcite cement (sample 87-20, 4.95% LDR twin strain, 12.47% PEV strain, 10.96% NEV strain); (c) transgranular extension veins (sample 87-22, 2.46% LDR twin strain); and (d) releasing bend in extensional microfault (sample 87-17, 2.67% LDR twin strain).

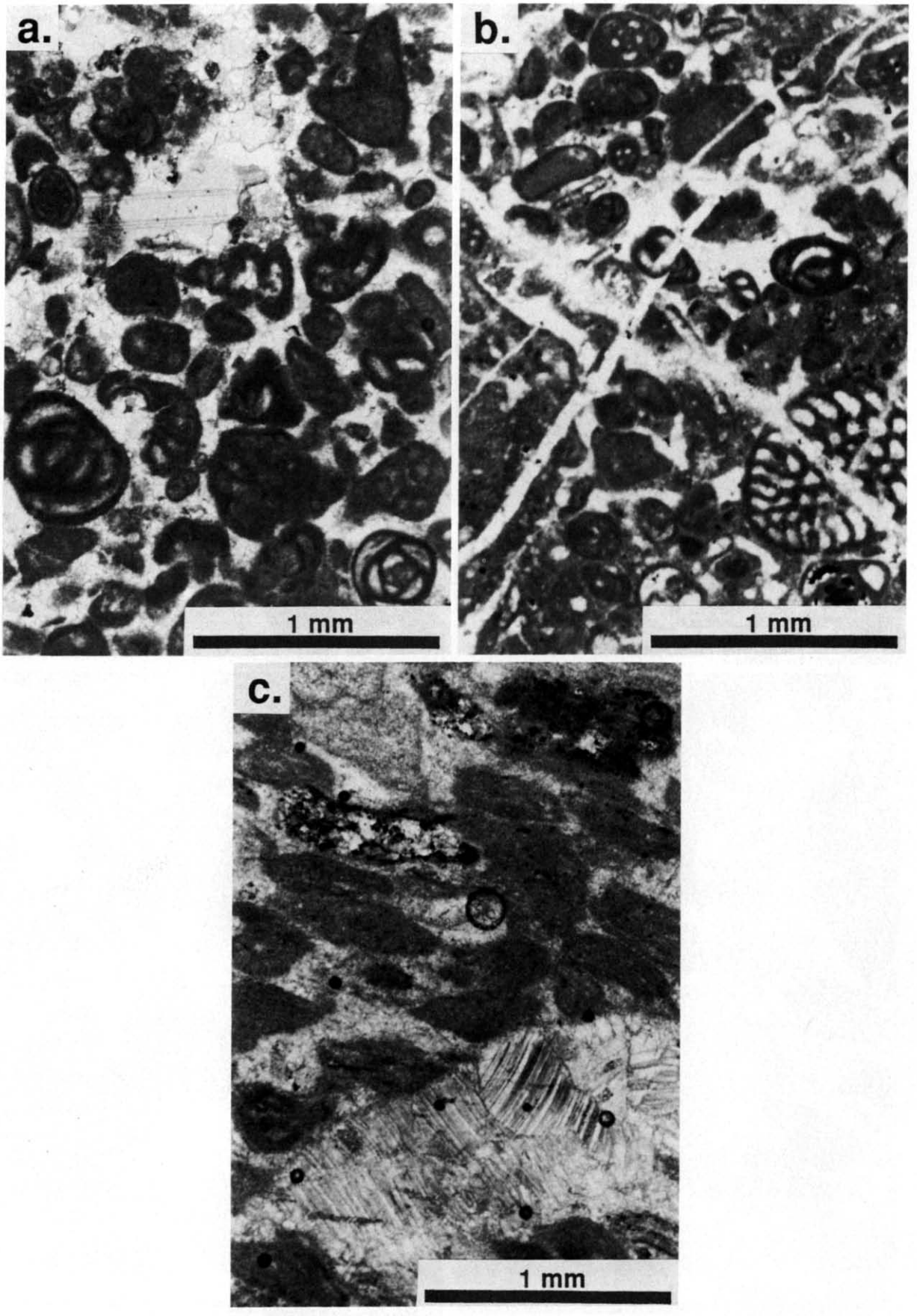

Fig. 5. Photomicrograph examples of: (a) uniform flow (sample 87-25, 0.28% LDR strain, DZ-2); (b) brittle (sample 87-27, 6.00% LDR strain, DZ-2) mode samples from the frontal portion of the fold–thrust belt; and (c) a uniform flow sample (sample 87-20, 4.95% LDR strain, 12.47% PEV strain, 10.95% NEV strain, AZ-5) from the internal part of the belt.

values may have experienced inhomogeneous or non-coaxial strain. Teufel (1980) used experimentally deformed limestone cylinders that were deformed by two non-coaxial shortening events (45° and 90° to each other) to test the calcite strain gauge technique for separating strain events. The two superposed strains were distinguishable using the calcite strain gauge by separating the PEV and NEV data from the original data set. The negative expected values in the original strain-gauge calculation for the experimentally deformed samples were greater than 40% (Teufel 1980). For the Subalpine Chain samples, the PEV and NEV strains may record individual twin strain events within a complex strain history.

Twinning in samples from diagenesis zones 2 and 3 are characterized by thin twins which have no microscopically visible width of twinned material but instead appear as thin dark lines. Twinning in the anchizone samples is dominated by thick twins which have measurable widths of twinned material and different extinction than host grain, however thin twins are also present and were measured. The diagenesis zone 4 sample appears to be in transition between thick and thin twinning. At temperatures below 150–200°C (DZ-4; *Ro* 1.6–2.6), increasing strain apparently occurred by the formation of new thin twins. Above the transition temperature, increasing strain mostly occurred by twin widening (Ferrill 1991a).

Deformation-mechanism associations

A deformation-mechanism association is defined by Groshong (1988) as "the deformation mechanisms formed under the same environmental conditions in the same rock type". Twenty of the 29 limestone samples from the northern Subalpine Chain belong to association II (brittle-framework deformation) (Table 3), in which strain due to crystal-plastic glide (e.g. twinning in calcite) is in the range of 0–2% and crystal truncation occurs by extension fracture or faulting (IIF), pressure solution (IIS) or both (IIFS) (Groshong 1988). Eight samples belong to association III (semi-brittle-framework deformation), in which crystal-plastic glide is obvious (2–15% strain) and mineral truncation may occur by faulting or extension fracturing (IIIF), pressure solution (IIIS) or both (IIIFS). In this paper, the terms F and S are only used when more than 3% of the grains are cut by extension fractures or faults (F) or pressure-solution surfaces (S). One sample (87-21) belongs to association IVG (glide tectonites) because the grain boundaries are visible and the crystal-plastic strain is more than 15% (PEV and NEV). The distribution of the deformation-mechanism associations is illustrated in Fig. 3.

Deformation modes and deformation conditions

The microstructural deformation mode diagram (Fig. 6) illustrates the deformation modes for the northern Subalpine Chain samples and reveals that 18 of the limestone samples deformed by the uniform flow mode (Fig. 7) at the thin-section scale and 11 samples deformed by the brittle faulting or extension fracture modes (Fig. 8). The deformation mode and prefailure strain are used to constrain the confining pressure and depth of thin-section scale deformation between surface and maximum burial conditions by plotting the uniform flow samples (Fig. 7) and brittle faulting and extension fracture mode samples (Fig. 8) on strain vs confining pressure deformation mode diagrams. The uniform flow samples did not fail at the thin-section scale and therefore are interpreted to have deformed at depths greater than those defined by the ductility curve for a given strain magnitude. The implication of the deformation mode for the brittle faulting and extension fracture samples is that failure occurred (i.e. a drop in stress occurred), however this cannot by proven unequivocally.

For the uniform flow samples, the bars representing the twin strain magnitudes and ranges of maximum burial conditions (Table 1) generally plot within the uniform flow field on the strain vs confining pressure deformation mode diagram (Fig. 7). Several of the dashed bars which denote PEV and NEV strains overlap the ductility curve. The uniform flow samples reached twinning strains (calculated using the LDR procedure) of 0.24–12.48% (up to 17.25 and 16.97% for PEV and NEV calculations, respectively) without brittle failure at the thin-section scale (e.g. Figs. 5a & c). By using the minimum pre-failure strains of the uniform flow samples, minimum depths of deformation can be interpreted from the ductility curve (Fig. 7). For example, according to the ductility curve, deforming to 12.48% strain (LDR; sample 87-21) without failure is

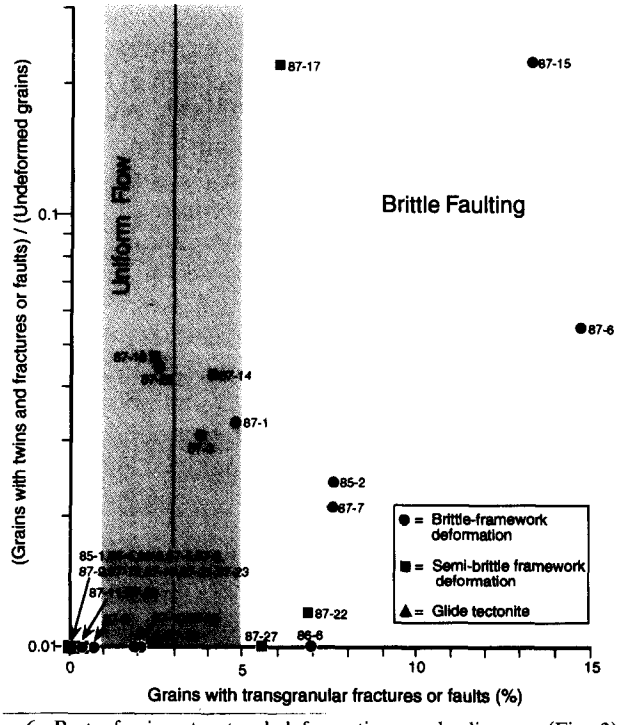

Fig. 6. Part of microstructural deformation mode diagram (Fig. 2) enlarged with Subalpine Chain data (Table 3) plotted to define macroscopic deformation modes for the samples.

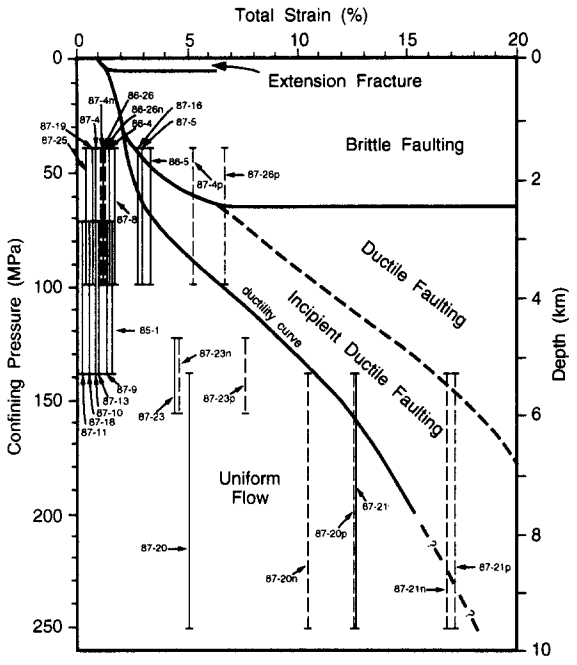

Fig. 7. Uniform flow samples from northern Subalpine Chain. Vertical bars for each uniform flow sample represent the estimated range of maximum confining pressure (Table 1) and twin strain (Table 3) on the experimental deformation mode diagram (Fig. 1, rotated) of Donath *et al.* (1971) and Tobin & Donath (1971). Dashed bars labeled p and n represent PEV and NEV calcite twin strains, respectively. The ductility curve gives the minimum confining pressure of deformation at which a given strain magnitude could be reached before brittle failure occurred. The minimum confining pressure of deformation (estimated from the ductility curve) and the maximum confining pressure (based on metamorphic grade; Table 1) bracket the confining pressure during deformation.

only expected at a confining pressure of 157 MPa or greater (Fig. 7), or at a depth of at least 6.0 km (assuming 26.0 MPa km^{-1}). If the PEV strain calculation for sample 87-21 (17.25%) is used instead, then a minimum confining pressure of 230 MPa is predicted, corresponding to a minimum depth of deformation of 8.9 km. For sample 87-20, the PEV strain of 12.47% without failure leads to the prediction of a minimum confining pressure at the time of deformation of 157 MPa, corresponding to a depth of 6.0 km. Therefore, according to the deformation mode (uniform flow), the minimum strains without failure, and the ductility curve on the confining pressure vs strain graph (Fig. 7), it is estimated that the two anchizone samples (87-20 and 87-21) deformed at the thin-section scale at depths greater than 6.0 km. The maximum possible depth of deformation is estimated using the peak metamorphic temperature for these samples of 300°C, a surface temperature of 10°C and a geothermal gradient of 30°C km^{-1} to be 9.7 km (Table 1).

The sample from DZ-4 (87-23) has a LDR twin strain of 4.41%, and PEV and NEV twin strains of 7.52 and 4.66%, respectively. Minimum confining pressures estimated using the strain magnitudes ductility curve (Fig. 7) are 82 MPa for the LDR strain, 108 MPa for the PEV strain and 83 MPa for the NEV strain. The corresponding estimated depths for these three confining pressures (assuming 26.0 MPa km^{-1}) are 3.2, 4.2 and 3.2 km, respectively. The estimated maximum depth at the time of peak metamorphism for samples 87-23 is 4.7–6.0 km (Table 1). Therefore, the internal deformation of the DZ-4 sample is interpreted to have occurred at a depth between 3.2 and 6.0 km.

The 15 uniform flow samples from DZ-2 and DZ-3 have LDR twin strains between 0.24 and 3.21% and PEV strains up to 6.59%. Using these strains and the ductility curve on the confining pressure vs strain deformation mode diagram yields minimum confining pressures of approximately 0–100 MPa, or depths of approximately 0–3.9 km (Fig. 7). The maximum depth estimated for samples from DZ-2 is between 2.7 and 3.8 km, and for DZ-3 is between 4.7 and 5.3 km (Table 1 and Fig. 9).

The extension fracture and brittle faulting data do not relate to the confining pressure–strain deformation mode diagram in a simple way. Of the 11 samples that deformed in the extension fracture or brittle faulting modes (Fig. 8), the bar representing maximum burial conditions for only one sample (87-27) crosses the ductility curve (Fig. 8) into the extension fracture or brittle faulting fields where the data are expected to plot at the time of failure. The vertical bars that represent estimated maximum depths (Table 1) for the remaining 10 samples plot on Fig. 8 in the uniform flow field. This suggests that either failure did not occur at the estimated maximum depth but occurred instead at a shallower depth, or that the effective confining pressure was significantly lower than that expected for the burial depth. Twins are found in all coarse calcite-filled extension veins which indicates that at least some twinning

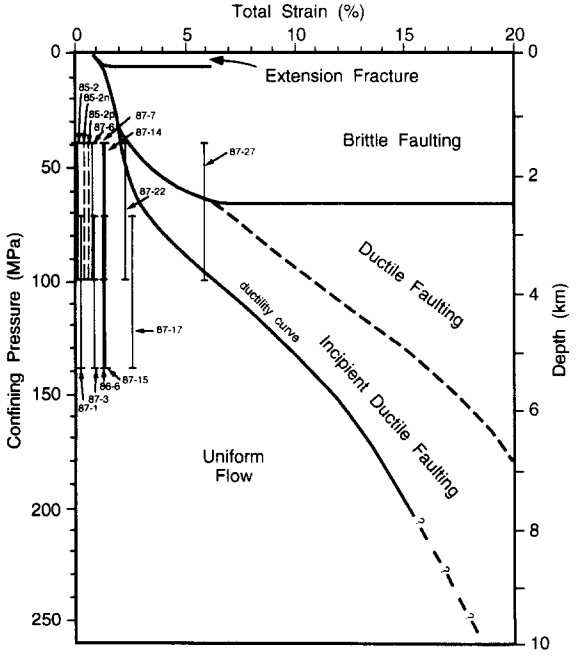

Fig. 8. Brittlely-deformed samples (extensional fracture or brittle faulting) samples from northern Subalpine Chain. Vertical bars represent the estimated range of maximum confining pressure (Table 1) and twin strain (Table 3) on the experimental deformation mode diagram (Fig. 1, rotated). Failure probably occurred at shallow depths or during lowered effective confining pressure due to high pore fluid pressure.

occurred after vein formation. This is similar to observations from the frontal part of the Helvetic Alps (Upper Glarus nappe complex) where measured twin strains are similar in magnitude and orientation for veins and sparry calcite cement, indicating formation of the veins before twinning (Groshong *et al.* 1984a). Twinned veins in samples from the Pine Mountain thrust sheet (southern Appalachians) record different strain orientations than the host due to non-coaxial twinning before and after vein formation (Kilsdonk & Wiltschko 1988). The twin strains for the Subalpine Chain samples may overestimate the prefailure strains for vein formation if the host rock continued to twin after vein formation. Assuming that the measured twin strain values are equal to or greater than the prefailure strains, the maximum confining pressures at the time of failure by extensional fracturing or brittle faulting are estimated from the ductility curve (Fig. 8) to be in the range of 0–50 MPa or maximum depths at the time of failure between 0 and 1.9 km (Fig. 8). Failure in sample 87-27 may have occurred at a confining pressure of as much as 62 MPa, or a depth of about 2.4 km. According to the deformation mode diagram, failure by brittle faulting at a depth of 2.4 km would require progressive deformation beginning in the uniform flow mode and continuing through the incipient ductile faulting mode to brittle faulting. There is no microstructural evidence to suggest that the rock deformed by incipient ductile faulting on the way to brittle faulting. Therefore, sample 87-27 also probably failed at a lower effective confining pressure than that predicted for maximum burial (Fig. 8).

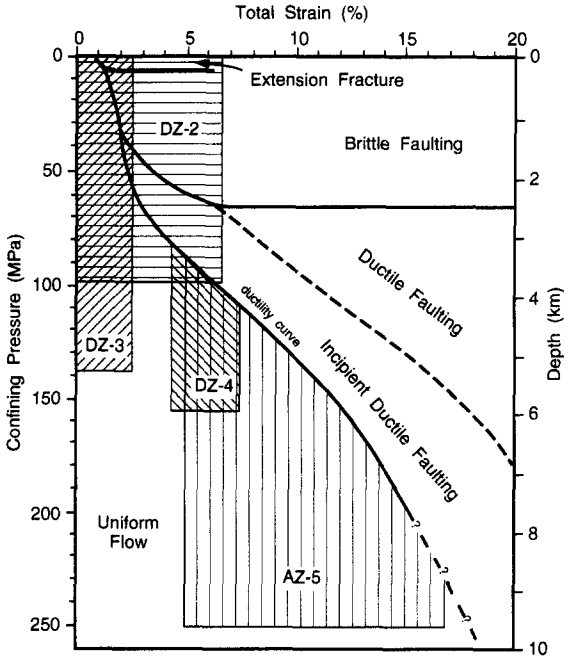

Fig. 9. Boxes illustrate the probable confining pressure during the thin-section scale deformation of all samples from the northern Subalpine Chain. The boxes are constrained by the deformation mode and twin strain, and the estimated maximum depths from Table 1.

DISCUSSION

In general, the minimum confining pressure estimates from the deformation mode, strain and ductility curve (on the confining pressure–strain deformation mode diagram) for the uniform flow samples show changes that are consistent with the lateral and across-strike changes in metamorphism in the fold–thrust belt (Fig. 9). The general increase of confining pressure and depth at the time of the uniform flow deformation in the external-to-internal direction across the northern Subalpine Chain is further supported by the previously discussed transition from dominant thin twinning to dominant thick twinning related to the temperature of deformation (Ferrill 1991a).

There are two obvious possibilities for explaining the low (effective) confining pressures of deformation for the brittlely deformed samples. First, elevated fluid pressure may have lowered the effective confining pressure (Secor 1965), leading to failure at depths greater than those predicted for failure by the ductility curve on the confining pressure–strain deformation mode diagram. Porosity was not observed in the samples. Fossils and cement are equally deformed by twins, fractures and faults which suggests that the cementation generally preceded failure. However, the pressure-solution surfaces seen in the samples indicate the presence of aqueous fluid in the rock during deformation. High-pressure fluid associated with adjacent shale strata or faults also cannot be eliminated as a possible cause of the brittle failure.

Second, failure at shallow depth could have occurred relatively early or late in the burial (tectonic or sedimentary) and exhumation history, before and/or after maximum burial. Point counts indicate that the twinning occurrence in the vein calcite is similar to that of the host grains, suggesting that veins may have formed relatively early, prior to maximum burial.

CONCLUSIONS

Thin-section scale deformation of limestone from the northern Subalpine Chain occurred by uniform flow and brittle faulting or extensional fracturing. The samples that deformed by uniform flow deformed mostly by twinning at minimum depths, estimated from the deformation mode and twin strain, of 0 to about 6.0 km, and maximum depths estimated from peak metamorphic data to be in the range of 2.7 to about 9.7 km. For the samples that contain extension fractures or faults, part of the twinning strain occurred after failure, as indicated by twinned calcite in extension veins. For these samples, the deformation mode and twin strain provide an estimate of the maximum depth at the time of brittle failure. The position of the ductility curve on the confining pressure–strain deformation mode diagram predicts brittle failure (vein formation and faulting) only at shallow depths (<2.4 km) for the generally low strains measured in the samples. However, the metamorphic data indicate that these samples were probably buried to depths of between 2.7 and 5.3 km, depths probably too

great for failure without involvement of elevated pore fluid pressure. The failure, therefore, probably occurred during relatively shallow burial (<2.4 km) or under conditions of lowered effective confining pressure due to high fluid pressures.

Acknowledgements—Field sampling for this study was supported by a research grant from The University of Alabama Student Government Association. Laboratory work was supported by grants from the Geological Society of America and ARCO, and two summer research fellowships from the University of Alabama Graduate Council. Thanks to Alastair Welbon for his field support and Mark Evans for his version of the calcite strain-gauge program. We thank D. Joe Benson, Benjamin A. Ferrill, Deborah Spratt, Harold Stowell, Bryan Tapp, William A. Thomas and Steven F. Wojtal for their valuable reviews that significantly improved the manuscript. This paper is a part of D. A. Ferrill's Ph.D. dissertation at the University of Alabama.

REFERENCES

Aprahamian, J. & Pairis, J.-L. 1981. Very low grade metamorphism with a reverse gradient induced by an overthrust in Haute-Savoie (France). In: *Thrust and Nappe Tectonics* (edited by McClay, K. & Price, N. J.). *Spec. Publs geol. Soc. Lond.* **9**, 159–165.

Barr, T. D. & Dahlen, F. A. 1989. Brittle frictional mountain building 2. Thermal structure and heat budget. *J. geophys. Res.* **94**, 3923–3947.

Burkhard, M. 1993. Calcite twins, their geometry, appearance and significance as stress–strain markers and indicators of tectonic regime: a review. *J. Struct. Geol.* **15**, 351–368.

Burkhard, M. & Kalkreuth, W. 1989. Coalification in the northern Wildhorn nappe and adjacent units, western Switzerland. Implications for tectonic burial histories. *Int. J. Coal Geol.* **11**, 47–64.

Carter, N. L. & Raleigh, C. B. 1969. Principal stress directions from plastic flow in crystals. *Bull. geol. Soc. Am.* **80**, 1231–1264.

Charollais, J., Pairis, J.-L. & Rosset, J. 1977. Compte rendu de l'excursion de la Société Géologique Suisse en Haute-Savoie (France) du 10 au 12 octobre 1976. *Eclog. geol. Helv.* **70**, 253–285.

Collet, L. W. 1927. *The Structure of the Alps*. Edward Arnold, London.

Dobrin, M. B. 1976. *Introduction to Geophysical Prospecting*. McGraw-Hill, New York.

Donath, F. A. 1970. Some information squeezed out of rock. *Am. Scientist* **58**, 54–72.

Donath, F. A., Faill, R. T. & Tobin, D. G. 1971. Deformation mode fields in experimentally deformed rock. *Bull. geol. Soc. Am.* **82**, 1441–1462.

Donath, F. A. & Fruth, L. S., Jr. 1971. Dependence of strain-rate effects on deformation mechanism and rock type. *J. Geol.* **79**, 347–371.

Dunnet, D. 1969. A technique of finite strain analysis using elliptical particles. *Tectonophysics* **7**, 117–136.

Engelder, T. 1985. Loading paths to joint propagation during a tectonic cycle: an example from the Appalachian Plateau, U.S.A. *J. Struct. Geol* **7**, 459–476.

Evans, M. A. & Dunne, W. M. 1991. Strain factorization and partitioning in the North Mountain thrust sheet, central Appalachians, U.S.A. *J. Struct. Geol.* **13**, 21–35.

Ferrill, D. A. 1991a. Calcite twin widths and intensities as metamorphic indicators in natural low-temperature deformation of limestone. *J. Struct. Geol.* **13**, 667–675.

Ferrill, D. A. 1991b. Curvature development and limestone deformation in the northern Subalpine Chain (Haute-Savoie, France). Unpublished Ph.D. dissertation, University of Alabama, U.S.A.

Ferrill, D. A. & Groshong, R. H., Jr. 1993. Kinematic model for the curvature of the northern Subalpine Chain, France. *J. Struct. Geol.* **15**, 523–541.

Frey, M. 1986. Very low-grade metamorphism in the Alps—an introduction. *Schweiz. miner. petrogr. Mitt.* **66**, 12–27.

Fry, N. 1979. Random point distributions and strain measurement in rocks. *Tectonophysics* **60**, 89–105.

Goguel, M. J. 1966. Carte Géologique de la France @ 1:80,000, feuille Albertville. Bureau de Recherches Géologiques et Minieres, Orléans.

Groshong, R. H., Jr. 1972. Strain calculated from twinning in calcite. *Bull. geol. Soc. Am.* **82**, 2025–2038.

Groshong, R. H., Jr. 1974. Experimental test of least-squares strain gage calculation using twinned calcite. *Bull. geol. Soc. Am.* **85**, 1855–1864.

Groshong, R. H. Jr. 1975. Strain, fractures, and pressure solution in natural single-layer folds. *Bull. geol. Soc. Am.* **86**, 1363–1374.

Groshong, R. H., Jr. 1988. Low-temperature deformation mechanisms and their interpretation. *Bull. geol. Soc. Am.* **100**, 1329–1360.

Groshong, R. H., Jr, Pfiffner, O. A. & Pringle, L. R. 1984a. Strain partitioning in the Helvetic thrust belt of eastern Switzerland from the leading edge to the internal zone. *J. Struct. Geol.* **6**, 5–18.

Groshong, R. H., Jr, Teufel, L. W. & Gasteiger, C. 1984b. Precision and accuracy of the calcite strain-gage technique. *Bull. geol. Soc. Am.* **95**, 357–363.

Guthrie, J. M., Houseknecht, D. W. & Johns, W. D. 1986. Relationships among vitrinite reflectance, illite crystallinity, and organic geochemistry in Carboniferous strata, Ouachita Mountains, Oklahoma and Arkansas. *Bull. Am. Ass. Petrol. Geol.* **70**, 26–33.

Hancock, P. L. 1985. Brittle microtectonics: principles and practice. *J. Struct. Geol.* **7**, 437–457.

Handin, J. 1966. Strength and ductility. *Mem. geol. Soc. Am.* **97**, 223–289.

Heard, H. C. 1963. The effect of large changes in strain rate in the experimental deformation of the Yule marble. *J. Geol.* **71**, 162–195.

Hyndman, D. W. 1985. *Petrology of Igneous and Metamorphic Rocks* (2nd edn). McGraw-Hill, New York.

Jaeger, J. C. & Cook, N. G. W. 1979. *Fundamentals of Rock Mechanics* (3rd edn). Chapman & Wood, London.

Kilsdonk, B. & Wiltschko, D. V. 1988. Deformation mechanisms in the southeastern ramp region of the Pine Mountain block, Tennessee. *Bull. geol. Soc. Am.* **100**, 653–664.

Kübler, B., Pittion, J. L., Heroux, Y., Charollais, J. & Weidmann, M. 1979. Sur le pouvoir réflecteur de la vitrinite dans quelques roches du Jura, de la Molasse et des Nappes préalpines, helvétiques et penniques. *Eclog. geol. Helv.* **72**, 347–373.

Mosar, J. 1988. Structures, déformation et métamorphisme dans les Préalpes Romandes (Suisse). Unpublished Ph.D. dissertation, University of Neuchâtel, Switzerland.

Mosar, J. 1989. Déformation interne dan les Préalpes medianes (Suisse). *Eclog. geol. Helv.* **82**, 765–793.

Plas, L. V. D. & Tobi, A. C. 1965. A chart for judging the reliability of point counting results. *Am. J. Sci.* **263**, 87–90.

Ramsay, J. G. & Huber, M. I. 1984. *The Techniques of Modern Structural Geology, Volume 1: Strain Analysis*. Academic Press, London.

Ricour, J., Rosset, J. & Schneegans, D. 1969. Carte Gélogique de la France @ 1:80,000, feuille Annecy. Bureau de Recherches Géologique et Minieres, Orléans.

Rutter, E. H. 1974. The influence of temperature, strain rate and interstitial water in the experimental deformation of calcite rocks. *Tectonophysics* **22**, 311–334.

Sawatzki, G. 1975. Étude géologique et minéralogique des flyschs à grauwackes volcaniques du synclinal de Thones (Haute-Savoie, France). Grès de Taveyanne et grès du Val d'Illiez. *Arch. Sc. Geneve* **28**, 265–368.

Secor, D. T. 1965. Role of fluid pressure in jointing. *Am. J. Sci.* **263**, 633–646.

Spang, J. H. & Groshong, R. H., Jr. 1981. Deformation mechanisms and strain history of a minor fold from the Appalachian Valley and Ridge Province. *Tectonophysics* **72**, 323–342.

Teichmüller, M. 1987. Recent advances in coalification studies and their application to geology. In: *Coal and Coal-bearing Strata: Recent Advances. Spec. Publs geol. Soc. Lond.* **32**, 127–169.

Teufel, L. W. 1980. Strain analysis of experimental superposed deformation using calcite twin lamellae. *Tectonophysics* **65**, 291–309.

Tobin, D. G. & Donath, F. A. 1971. Microscopic criteria for defining deformation modes in rock. *Bull. geol. Soc. Am.* **82**, 1463–1476.

Turner, F. J. 1953. Nature and dynamic interpretation of deformation lamellae in calcite of three marbles. *Am. J. Sci.* **251**, 276–298.

Wu, S. 1989. Strain partitioning and deformation mode analysis of the normal faults at Red Mountain, Birmingham, Alabama. *Tectonophysics* **170**, 171–182.

Yonkee, W. A., Parry, W. T., Bruhn, R. L. & Cashman, P. H. 1989. Thermal models of thrust faulting: Constraints from fluid-inclusion observations, Willard thrust sheet, Idaho–Utah–Wyoming thrust belt. *Bull. geol. Soc. Am.* **101**, 304–313.